H·E·S·S·-II: Expansion of H·E·S·S· for higher sensitivity and lower energy

Michael Punch for the HESS Collaboration
Astrophysique et Cosmologie (APC),
UMR 7164 (CNRS, Université Paris VII, CEA, Observatoire de Paris)
Collège de France, 11 Place Marcelin Berthelot, F-75231 Paris Cedex 05, France

The H·E·S·S· (High Energy Stereoscopic System) collaboration is pursuing plans to expand the current Phase-I array of four Imaging Atmospheric Cherenkov Telescopes (IACTs) with the addition of a very large Cherenkov telescope (VLCT) at the centre of the array, for observation of galactic and cosmic sources of Very High Energy (VHE) gamma rays, with a significant improvement in sensitivity over, and a detection threshold below, that of previous IACTs. The design concerning the mechanics, optics, and electronics, in particular detailing the improvements based on the experience gained with H·E·S·S·-I, is described. The expected performance of H·E·S·S·-II, alone and in conjunction with the H·E·S·S·-I array, based on detailed Monte Carlo simulations is shown.

1 The H·E·S·S· Telescope System

The H·E·S·S· detector for observation of > 100 GeV γ-rays has been operating since June, 2002 (beginning with a single IACT) in the Khomas highlands of Namibia (23° S, 15° E, 1.8 km a.s.l.). It was constructed by an international collaboration from Germany, France, Britain, Ireland, the Czech republic, Armenia, South Africa, and the host country, Namibia. It is the first large-scale IACT system with a stereoscopic trigger and fast electronics, and so has unparallelled sensitivity in the domain above 100 GeV.

The detector system consists of four IACTs in a square of side 120 m. Each telescope mount has a tessellated mirror dish of area 107 m^2 (380 Ø 60 cm facets), with a Cherenkov imaging camera in the focal plane at 15 m. The mounts have a pointing precision of 8" with a slew rate of $100°/\mathrm{min}$., while the mirror PSF is 1.4' (80% containment radius). The camera contains 960 photo-multipliers (PMs) with 0.16° pixel-size, for a 5° field of view. Each PM is equipped with a "Winston cone" light guide to minimize dead-space between the PM sensitive areas and to cut down

on albedo light (not coming from the mirror). Further details of the optical structure are given in [1, 2].

The read-out electronics are all contained within the camera (which fits in a cube of side $1.5\ \mathrm{m}$, weighing $900\ \mathrm{kg}$). The modular construction of the cameras (60 "drawers" each of 16 PMs) permits their maintenance at this remote site. The read-out of the camera is triggered when the signal from a number of PMs exceeds a trigger threshold in an effective $\sim 1.3\ \mathrm{ns}$ trigger window. The PM signals, which are stored in an analogue memory while awaiting the trigger, are then read out, digitized, and integrated within a $16\ \mathrm{ns}$ window. The results are then sent from the camera's on-board data-acquisition system to the control room via optical fibres. In stereoscopic operation, the stereo trigger rate is $\sim 350\ \mathrm{Hz}$ for current trigger conditions.

Phase-I of H·E·S·S· was fully completed in December, 2003, with the addition of the fourth telescope, since which time the system has been operating at its full sensitivity. The energy threshold of the system is $\sim 100\ \mathrm{GeV}$ at the trigger level for sources close to Zenith, or $\sim 120\ \mathrm{GeV}$ after background rejection cuts with an angular resolution of up to 0.06° (from 0.1° with a single telescope) and allowing spectral measurements with an energy resolution of $\simeq 15\%$. See [3, 4] for further details of the H·E·S·S·-I system. The sensitivity of the H·E·S·S·-I system has been confirmed by observations of the Crab Nebula; for sources close to Zenith, 1 Crab-level sensitivity (5σ detection) in only 30 seconds (or 1% Crab in 25 hrs) is achieved. This performance has permitted the detection of many new sources of γ-rays, including supernova remnants, active galactic nuclei (AGN), pulsars in binary systems, and unidentified sources, and has led to the catalogue of VHE sources being more than tripled by H·E·S·S·.

2 Addition of the Very Large Cherenkov Telescope for H·E·S·S·-II

The major motivation for the next step by the H·E·S·S· collaboration is provided by the advent of the GLAST satellite-borne detector, to be launched in 2007, which will provide an unparallelled measurement of the gamma-ray sky at lower energies (10 MeV–100 GeV), so inciting the construction of an IACT with increased sensitivity and lower threshold to bridge the gap between these energy ranges. This can be achieved by the addition of a Very Large Cherenkov Telescope (VLCT) at the centre of the current array in Namibia as shown in the photomontage in figure 1. Table 4 shows the improvements planned for the VLCT over H·E·S·S·-I.

Such a system, combining a VLCT and the current H·E·S·S·-I array, will give access to an energy range which will allow wider energy coverage of already-known sources, and will give access to new categories of sources. More distant AGNs can

be detected, without the difficulty of γ-ray absorption on the intervening intergalactic background light. The emission from pulsars, which cuts off at some energy between current satellite measurements and the IACT range, can be measured; the energy of this cut-off is strongly dependent on the emission models. For the known sources, measurement over a wider energy range will permit emission models to be tested in greater detail. The greater sensitivity of such a system will allow shorter time-scale variability to be measured for variable sources such as AGNs or binary systems, providing key information on the emission region size and location.

Figure 1: Photo of the current four-telescope H·E·S·S· Phase-I array, with an artist's impression of the Phase-II 28m Ø telescope (VLCT) in the centre of the array superimposed.

2.1 Structure

As for H·E·S·S·-I telescopes, the telescope structure for the VLCT will be a steel space-frame structure with an alt-azimuthal mount. The mount (azimuthally rotating section) is a space frame supporting two A-frame structures which hold the elevation bearings. This is driven in azimuth by a drive system of six bogies, with four wheels each, running on a circular rail of 36 m diameter about a central pintle bearing which supports the horizontal forces due to wind loading. Four of the bogies are driven, with two driven wheels per bogie. The range of rotation is $540°$, with a slew rate of $200°/\mathrm{min}$.

The dish support structure is a deep space frame which supports the dish at four points on the dish's rear side, chosen to minimize deformations of the dish shape, and which rotates about its horizontal axis around the elevation bearings. The elevation drive consists of two motors, attached to the azimuth structure by long beams, powering gears which run on arcs of circles (rack and pinion system vs. friction bearings for H·E·S·S·-I) which are attached to the dish support structure, with a range from $-35°$

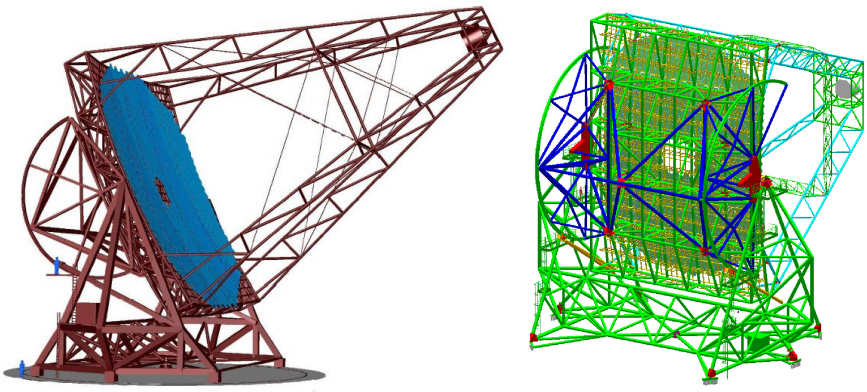

Figure 2: (a) Artist's view of the very large Cherenkov telescope (b) isometric view of from the rear of the telescope, showing the mount, dish support structure (darker colour), dish, and camera support quadrupod.

(with the camera on the ground) to 180° (looking 'backwards', for ease of mirror installation).

The camera is held in the focal plane by a quadrupod attached to the four four corners of the dish. Each quadrupod leg is a space-frame, stiffened by a set of connecting braces, giving only about 7.7% shadowing of the incoming light.

The drive positions are controlled with encoders, used for the on-line tracking for a deviation of about 1" RMS between the nominal and actual encoder precision. Offline corrections to compensate encoder offsets and encoder nonlinearities and the bending of the camera arms are applied to the databased on the data from the guide telescope and from the CCD camera monitoring the bending of the camera arms via positioning LEDs on the PM camera for an accuracy of 5–10" absolute pointing.

The total weight of the structure, including the facets, supports, and camera, will be approximately 560 tonnes, with a height of $\sim 40\,\mathrm{m}$ when the optical axis is in the horizontal position, and focal length of $36\,\mathrm{m}$. Design studies have been performed by MAN Technologie, indicating that such a structure will be able to respond to the specifications, with a tracking precision in the arc-minute range. Wind speeds of 50, 80, 120, and 160 km/h will be supported for operation, parking, rest at any position, and survival respectively. The surface accuracy of the dish is such that, at least up to 45° zenith angle, the surface will be stable within the optical specifications (0.15 mrad RMS) including wind loads and temperature effects.

2.2 Mirror Dish Design

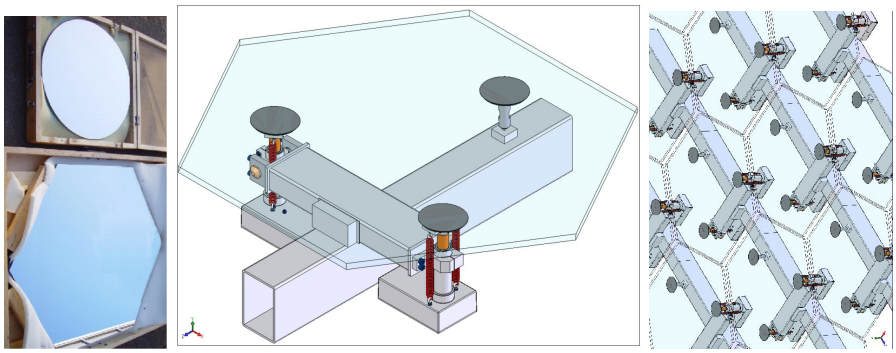

Figure 3: (a) Comparison photo of a H·E·S·S·-I mirror facet and a sample VLCT facet, (b) Mirror support and alignment units attached to a beam of the mirror support segment (c) array of facets on a mirror support segment.

The mirror will be a tessellated array of about 850 facets, combined to make a dish with a surface area of 596 m^2 (approximately $24\mathrm{m} \times 32\,\mathrm{m}$ width by height), with a parabolic contour since the standard Davies-Cotton design would have too great a time-dispersion for such a large dish. However, off-axis image performance for a parabolic dish is worse than the Davies-Cotton design for fixed f/D (in this case 1.2, with a focal length of 36 m), so the field of view is limited compared to H·E·S·S·-I.

The default option of the mirror facets is to have standard glass mirrors with aluminium reflective coating and quartz protective layer, with similar specifications as for H·E·S·S·-I. Other designs of mirror (e.g., vacuum-formed alanod honeycomb sandwich) are also being investigated to determine if they can meet specifications while providing cost advantages. Specifications are similar to H·E·S·S·-I, requiring that the diameter of a circle containing 80% of the reflected light for an incident parallel beam should not exceed 1 mrad, with a typical 80% diameter of 0.5 mrad or less, and with a reflectivity above 80% in the range 300–600 nm.

The facet size is a 90cm hexagon flat-to-flat (vs. 60cm circle for H·E·S·S·-I, see figure 3(a)), which will be mounted on an improved version of the three-point mountings in H·E·S·S·-I (see figure 3(b)), equipped with two actuators for alignment. A prototype of this improved mounting is already running. With a weight of 19 kgs per facet ($\sim 1.5\,\mathrm{cm}$ thickness for glass facets), a weight limit of 30 kg per mirror was assumed, including the alignment mechanism.

25 planar "mirror support segments" are mounted on the dish (5×5) so as to approximate the parabolic shape (max. deviation $\Delta z < 8\,\mathrm{cm}$). Each segment holds up to 42 facets (6×7). Before inserting the dish in the telescope mount the individual

mirror alignments units with cables are installed on these support segments. The facets will finally be attached to the alignment units just prior to camera installation.

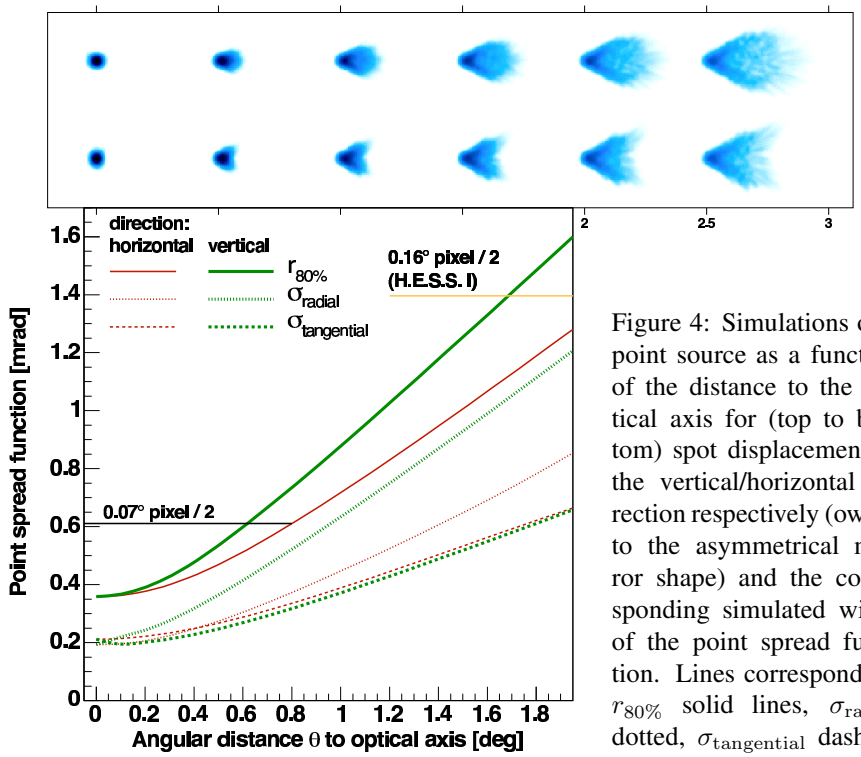

Figure 4: Simulations of a point source as a function of the distance to the optical axis for (top to bottom) spot displacement in the vertical/horizontal direction respectively (owing to the asymmetrical mirror shape) and the corresponding simulated width of the point spread function. Lines correspond to: $r_{80\%}$ solid lines, σ_{radial} dotted, $\sigma_{\mathrm{tangential}}$ dashed; the upper/lower lines in each case showing the PSF for the vertical/horizontal direction respectively. The radius of H·E·S·S·-I and VLCT pixels are shown for comparison.

Simulations indicate that, thanks to the large dish focal length relative to the facet size, the exact focal length of each facet does not need to be adapted to its position on the parabola, and even a single uniform focal length for all mirrors seems acceptable. The simulated spot size of the VLCT for a point source as a function of distance from the optical axis is shown in figure 4, together with different measures of the width of the point spread function.

2.3 Camera Design

The focal plane is 2m in diameter, for a full field of view of $3.17°$, taking into account the worse off-axis optical quality for the parabolic dish for the given focal length and in order to keep the number of pixels to a reasonable level. This is smaller than the $5°$ field of H·E·S·S·-I, since the physics goals are centred on point-like sources (AGNs, pulsars, binary systems...) for which the low-energy γ-rays fall closer to the centre of the field.

Each pixel of the focal plane detector is a PM for which the Cherenkov light is focused onto the photo-cathode by a Winston cone located in a hinged plate which pivots to cover the PM array. The same physical PM size is used as in H·E·S·S·-I, which combined with the same f/D allows an identical Winston cone design to be used (injection moulded polycarbonate half-cones with aluminization and SiO_2 protection), and incidentally gives the same Night-Sky Background (NSB) rate per pixel in the VLCT as in H·E·S·S·-I (100 MHz), so the PMs can operate at the same gain of 2×10^5. The Winston cone entrance aperture of $42\,\mathrm{mm}$ defines the pixel size, $0.07°$ (compared to $0.16°$ for H·E·S·S·-I). The smaller pixel angular size will give a better definition of the Cherenkov images, and so better angular resolution, and also will reduce the number of pixels which need to be turned off during operation due to stars in the field of view. The total weight of the camera, with integrated electronics, will be 2.5 to 3 tonnes, and would fit in a cylinder of length 2.2 m and diameter 2.5 m.

Camera Mechanics

The modular design of the camera mechanics and electronics used in H·E·S·S·-I is retained (see figure 2.3), with the PMs being grouped in "drawers" of 16 PMs. These 128 drawers are plugged-in to the focal plane, and a hinged plate containing the Winston cones pivots to cover the PM array or opens to allow drawer extraction. Behind the drawer assembly, fixed racks containing acquisition electronics are accessible from the read door and from two side doors. The pneumatic lid of the camera must be made in two parts, as a lid in a single part would be overly heavy if it were to have sufficient structural solidity. The camera will be mounted such that it can move by $\sim 10\,\mathrm{cm}$ along the optical axis, so that the telescope can be refocused to the shower maximum as a function of zenith angle.

Contrary to H·E·S·S·-I, the use of active cooling of the camera rather than simple ventilation is being studied. "Vortex" cooling systems enable a supply of air under pressure ($\sim 2\,\mathrm{bars}$, at between 12–20°C input) to be divided into two turbulent streams, one at raised temperature which is rejected, and another at a lower temperature which is injected in the camera when needed for cooling. The advantage of such a system would be to provide a supply of clean, dry air at constant temperature, thus simplifying characterisation of the camera and calibration, without dust or other par-

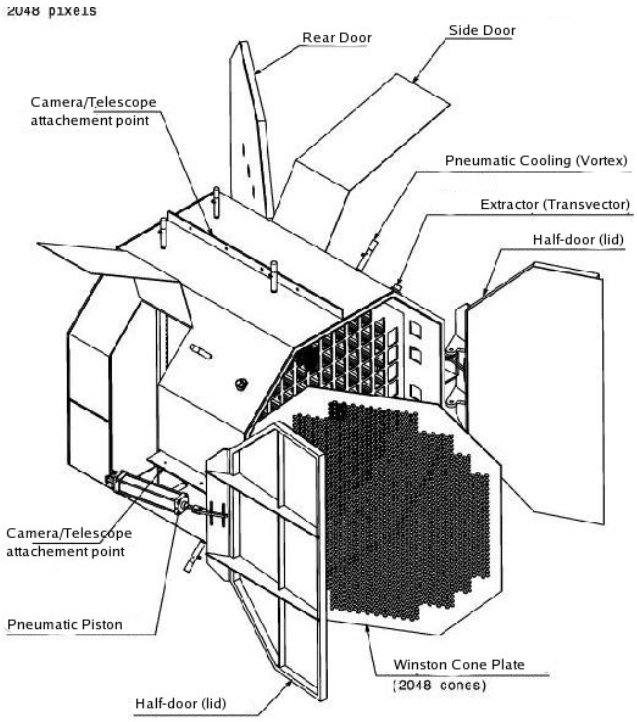

Figure 5: View of the camera mechanics with all doors open, showing the lid with two half-doors, the Winston cone plate, the pigeon-hole plate into which the drawers are plugged, and the side and rear access doors.

ticles, thus increasing the longevity of the electronics. Cooling tests are under way on a mini-camera equipped with 20 test drawers with the full mechanics and connectors, and with the equivalent heat output of the electronics provided by resistances. This mini-camera will also serve for the optical and electronics tests of the fully-assembled drawers.

Camera Electronics

Each drawer of 16 PMs contains an individual high-voltage supply system for each PM, the analogue memory for signal storage during the trigger formation time, some local trigger electronics, and analogue-to-digital conversion and buffering of the signals, along with all necessary slow control signals for setting thresholds, reading temperatures, etc. Behind the drawer assembly, fixed racks contain the power supplies for

all electronics (using switched power supplies with a single input to provide the low-voltage DC supplies), compact-PCI crates with the level-1 sector trigger electronics, trigger fanout and management, FIFO event buffers, GPS, and the data-acquisition (DAQ) CPUs, as well as the ethernet switches for communication with the control room.

PMs with improved performance over those used in H·E·S·S·-I (from Photonis) are being tested, with modifications to the entry window, the photo-cathode material, and the electron collection for improvement in the Cherenkov photon collection efficiency. A test bench for characterisation of sample PMs based on the H·E·S·S·-I electronics will be used for the final selection. The PM and electronics response is such that the single photo-electron (1 p.e.) peak can be distinguished; this is used as a calibration tool. The electronics dynamic range allows signals from 0.1–6000 p.e. to be measured, so giving a linear response even for the brightest pixels in showers up to ~ 10 TeV.

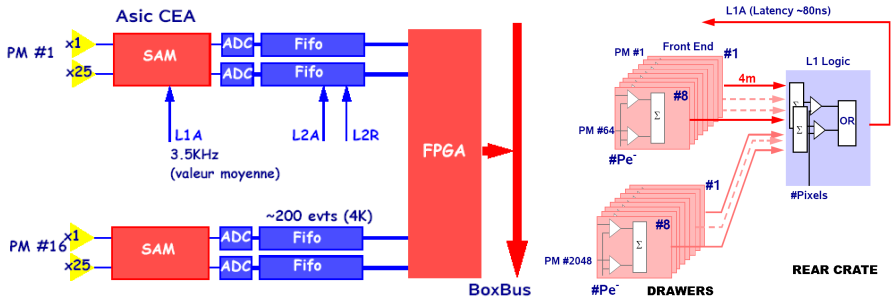

Figure 6: (a) The pipeline followed within the drawer by the signals for read-out, showing the amplification, analogue storage within the SAM, ADC conversion,event storage in the FIFO, and FPGA for formatting and transfer (b) The level-1 trigger logic, showing the analogue sums of the comparator outputs from 8 pixels performed withing the drawers, combined in the rear crate to give a trigger for a defined number of pixels over threshold in one of the overlapping sectors.

The key component of the electronics, which enables a compact, integrated camera containing all the trigger, conversion, and acquisition electronics to be built, is the "Swift Analogue Memory" (SAM), which is an updated version of the "Analogue Ring Sampler" memory (ARS0) used in H·E·S·S·-I, in this case designed specifically for the needs of Cherenkov astronomy by the SEDI-Saclay. The SAM allows the storage of the analogue signals from the PMs during the level-1 trigger formation time, after which the signals can be read and converted in a conventional, fast, ADC (i.e., not flash). The SAM contains two differential channels per chip, each of which permits analogue sampling and storage of the PM signals in an analogue ring buffer with

256-cell depth (implemented as a 16×16 matrix), at 1 GHz (variable from $500\,\mathrm{MHz}$ to $2\,\mathrm{GHz}$), with non-linearity $< 2\%$. The use of differential channels allows reduced noise and cross-talk reduced to $< 0.1\%$, with a bandwidth of 300 MHz at gain 1 (increased from 80 MHz in the ARS0), allowing faster rise-times to be sampled. All inputs and outputs are also in LVDS (low-voltage differential signalling). The noise-level of $< 0.8\,\mathrm{mV}$ for a maximum signal of $2\,\mathrm{V}$ gives an effective 11.3-bit dynamic range per channel. The read-out speed is more than ten times greater than for the ARS0 used in H·E·S·S·-I, so greatly reducing the dead-time; $1.6\,\mu\mathrm{s}$ per 16-cell block, with a maximum read speed greater than $400\,\mathrm{kHz}$. Power consumption will also be lower than for the ARS0 chip ($\sim 300\,\mathrm{mW}$), though for half the number of channels per chip. For cost, speed, and integration issues, the inclusion of ADCs within the SAM was considered, however the subsequent evolution in price and performance of the external components is such that this is not necessary, so the currently-working prototype will be used in the final design (with minor modifications), thus eliminating a major item on the schedule critical path. This component is described in greater detail in [6], these proceedings.

The signal from each PM is divided into three paths, first with a gain 1 sent to one channel of a SAM (the low-gain, LG, channel), the second with gain $\times 25$ sent to the other SAM channel (the high-gain, HG, channel), and the final path sent to the trigger electronics. Figure 6(a) shows the pipeline followed within the drawer in the conversion chain to the read-out. After read-out, the linear range for the LG channel has been measured to be 0.1–150 p.e., and that of the HG channel from below 15–6000 p.e. on the SAM test-bench using prototype electronics (see [6]).

The level-1 trigger design (see figure 6(b)) is the same as in H·E·S·S·-I, where the amplified signal (gain $\times 50$) from each PM is passed through a fast comparator, and an analogue sum of these signals is performed in a sector of 64 adjacent pixels (8×8), giving the number of pixels overlapping in time which have passed the comparator threshold in the sector. Since the comparator is fast, the equivalent trigger coincidence window is $\sim 1.3\,\mathrm{ns}$. Two sub-sums of 8 PMs are performed in each drawer, and these signals are sent to the rear crate sector-trigger electronics for overall level-1 trigger fabrication. To cover the entire camera, 99 overlapping sectors are used, and the level-1 trigger occurs if the summed signals in one of these sectors exceeds a pre-defined number of pixels. The level-1 trigger signal is fanned out to each drawer, where it triggers the read-out of the SAM. The trigger formation time is expected to be about $80\,\mathrm{ns}$, well within the SAM memory depth. Note that for a typical trigger configuration of 4 pixels above 3 p.e., an event rate of $\sim 3\,\mathrm{kHz}$ is expected from Monte Carlo simulations.

A level-2 trigger is being studied, in which the pattern or topology of pixels which pass a threshold level is used to reject events which are caused by the night-sky background light, and possibly also for the rejection of the events caused by isolated

muons falling near the telescope and large hadronic events. This level-2 trigger is slower than the level-1, $\sim 20\,\mu$s, and is used to reject events which are stored in the drawer FIFOs before summation and transmission (see below). These studies are described here in [5].

After each drawer has received a level-1 trigger signal, it begins conversion of the signals stored in the SAMs in a window about the event arrival time. A window length of up to $16\,$ns is used in H·E·S·S·-I to decrease the NSB; for the VLCT this may be decreased as the bandwidth has been improved. Each channel has its own ADC (contrary to the multiplexing of channels used in H·E·S·S·-I), and the ADC signals are stored in a digital FIFO per channel capable of holding 200 events (which is a further improvement on H·E·S·S·-I). If the level-2 trigger rejects the event, then it is abandoned from the FIFO before transmission, thus decreasing the dead-time. The FIFOs are read into the on-board FPGA (Field-Programmable Gate Array), which sums the signals in each window for transmission to the DAQ in the rear crates according to a message passing protocol on a custom-designed bus called "BoxBus". Unlike H·E·S·S·-I, the drawers are connected to this bus via a repeater, so reducing the cable load to $\sim 30\,$cm, except for the first drawer on the bus, thus minimizing transfer problems. The individual time-slices may also be transmitted in special test modes, though with a greatly increased dead-time due to the quantity of data transmitted. Contrary to H·E·S·S·-I, separate buses are used for data and slow-control signals, allowing greater flexibility.

The front-electronics can cope with an event rate up to 50 kHz with $< 10\%$ dead-time, however current technology allows network transmission and storage at a rate of about $4\,$kHz, to be compared to the expected event rate of $\sim 3\,$kHz without a level-2 trigger, or with a greater margin if the level-2 trigger is included.

This integrated camera is connected to the control room by a small number of cables; power, ethernet fibre for the data and control, and two fibres for the trigger signal (local telescope trigger out, for integration into the central trigger system of the array, and central trigger coincidence return signal). Integration of all the electronics in the camera thus simplifies the transfer of signals to the control room, as well as permitting a very fast level-1 trigger electronics in proximity to the PM signals, with the electronics being self-contained within a Faraday cage for EMI (electromagnetic interference) reduction.

3 Performance of the H·E·S·S· System

The very large Cherenkov telescope, placed at the centre of the array of H·E·S·S·-I, will have a free-running trigger which will allow it to run in mono-telescope mode for the lowest energy events. The events which are seen by the VLCT alone are the lowest-energy events, and give access to the energy range down to ~ 15–$25\,$GeV, but

with low background-rejection capability, and large energy and angular resolution.

The VLCT trigger signal will also be included in the central trigger system of H·E·S·S·-I, where the trigger signals from each telescope are put in time to account for the shower arrival direction and a coincident trigger if formed if two or more telescopes trigger within 80 ns. This will permit "hybrid" events, in which a coincidence between the VLCT and a single H·E·S·S·-I telescope will trigger the readout of the H·E·S·S·-I telescope in addition to the VLCT. This class of events will allow an intermediate energy range to be accessed, where the stereo coincidence will provide the angular origin on an event-by-event basis as for H·E·S·S·-I, with improved background rejection, and the increased number of Cherenkov photons in the VLCT image will provide reasonably good energy resolution.

Finally, the events which trigger two or more H·E·S·S·-I telescopes will be read out as before, and it is expected that all such events will also cause an independent trigger in the VLCT, giving an image with much finer resolution than in the H·E·S·S·-I telescopes and with a greater number of Cherenkov photons. Such an image will provide better angular and energy resolution for each stereoscopic event, and improve the background rejection capability, so improving the sensitivity of the H·E·S·S·-II system in the H·E·S·S·-I energy range by a factor of two or more.

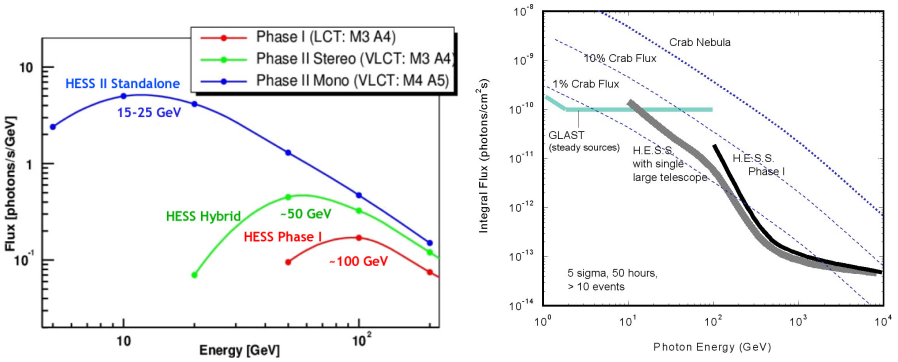

Figure 7: (a) Differential detection rate versus energy for the current H·E·S·S·-I system, for "hybrid" events, and for the VLCT in stand-alone mode. (b) Expected sensitivity based on simulations, showing the minimal detectable flux above a certain energy threshold. For H·E·S·S·-I, a significance of 5σ and at least 10 events in 50 hours observation time is required; for GLAST 1 year observing time is assumed. The Crab nebula flux is shown for reference.

Simulations of the H·E·S·S·-I system are successful in describing the measured event rate from hadronic and muon backgrounds. These simulations have been modified to include the VLCT, so the extrapolation to lower energy should be close to the

reality. When applied to gamma-ray simulations, the threshold response, defined as energy for which the maximum event rate for a Crab-like spectrum, yields a threshold of $\sim 50\,\mathrm{GeV}$ for the category of hybrid events in which the VLCT triggers in coincidence with a telescope of the H·E·S·S·-I system. In mono-telescope mode, the VLCT trigger threshold is of order 15–25 GeV, though the effective analysis threshold will be for these less-well defined events remains to be determined. This is to be compared with a trigger threshold of $\sim 100\,\mathrm{GeV}$ at Zenith for the current H·E·S·S·-I system, as can be seen in figure 7(a). The expected improvement in sensitivity, compared to H·E·S·S·-I, is shown in figure 7(b) together with the GLAST sensitivity, in comparison with the Crab nebula flux, demonstrating the complementarity of the two observing techniques.

4 Conclusions

The addition of a very large Cherenkov telescope (VLCT) to the centre of the current array of H·E·S·S·-I telescopes in Namibia will allow the threshold of the system to be greatly decreased (down to $\sim$ 15–25 GeV), thus opening up an energy range in which will, in addition to the targets which have already been detected and measured by H·E·S·S·-I (pulsar wind nebulæ, binary pulsar systems, active galactic nuclei, and unidentified sources) should provide access to new source categories such as pulsars, more distant AGNs, neutralino dark matter, as well as more extensive, sensitive measurements, with shorter time-scale variations, of the already-detected sources. The ambitious installation schedule, with operations beginning in the Summer of 2008, is based especially on the unique opportunity of observations in parallel with the GLAST satellite, which will be launched in Autumn, 2007, so providing a temporal and spectral overlap in the domain of very high energy gamma-ray astronomy.

References

[1] K. Bernlöhr et al., *Astroparticle Physics* **20**, 111 (2003)

[2] R. Cornils et al., *Astroparticle Physics* **20**, 129 (2003)

[3] W. Hofmann et al., *Proc. 28th ICRC* (Tsukuba) 2811 (2003)

[4] P. Vincent et al., *Proc. 28th ICRC* (Tsukuba) 2887 (2003)

[5] M. Tlucyzkont et al, *these proceedings pp. 509-517*

[6] P. Goret et al, *these proceedings pp. 501-507*

Item	H·E·S·S·-I	VLCT
Telescope Structure		
Dimension	12 m Ø dish	28 m equiv. Ø dish
Focal length	15 m	36 m
Elevation Drive	Friction Drive	Rack and Pinion
Azimuth speed	$100^\circ/\mathrm{min}$	$200^\circ/\mathrm{min}$
Total Weight	$20\,\mathrm{t}$	$560\,\mathrm{t}$
Dish and Mirrors		
Dish type	Davies-Cotton	Parabolic
Facet mounting	Mounted on structure	Pre-aligned Panels
# and type of facets	380×60 cm circular	850×90 cm hexagonal
Mirror area	$107\,\mathrm{m}^2$	$596\,\mathrm{m}^2$
Camera Structure		
Field of View	5°	3.17°
Pixel size	0.16° / 2.8 mrad	0.7° / 1.2 mrad
# Pixels	960 ($\times 4$ cameras)	2048
Cooling	Ventilation	Active Vortex cooling
Position	Fixed	Adjustable focus
Size / Weight	$\sim 1.5\,\mathrm{m}$ cube, $\sim 1\,\mathrm{t}$	$\sim 2.5\,\mathrm{m}$ Ø $\times 2.2\,\mathrm{m}$, $< 3\,\mathrm{t}$
Analogue Memory		
Techno	0.8μ	0.35μ
Channels/Chip	4 used	2
Memory depth	128 cells	256 cells
Channel type	Simple	Differential
Sampling speed	0.3–1 GHz	0.3–2 GHz
Bandwidth	80 MHz	300 MHz
Noise level / Dynamic Range	$2.5\,\mathrm{mV}$ / 9.8-bit	$< 0.8\,\mathrm{mV}$ / 11.3-bit
Dynamic Range (p.e.)	1600 p.e.	6000 p.e
Maximum readout speed	$60\mu\mathrm{s}$ / 17 kHz	$< 2\mu\mathrm{s}$ / $> 400\,\mathrm{kHz}$
Camera & readout		
# Drawers	60 ($\times 4$ cameras)	120
Trigger	Level-1 only (sector + timing)	Level-1 + Level-2 (topological)
Drawer Communication	Combined bus	Separate Data/Control buses
Drawer Communication	Custom bus	Custom bus, Active repeaters
Event buffering	Crate FIFO	Drawer & Crate FIFO
Drawer conversion time	$\sim 275\mu\mathrm{s}$	$20\mu\mathrm{s}$
Drawer-to-crate transfer	(in series with above) $\sim 185\mu\mathrm{s}$	(in parallel) $\sim 20\mu\mathrm{s}$
Network/Storage speed	$\gg$ evt rate (2.34 k.evts/s)	$\sim$4 k.evts/sec
Front-end deadtime	$\sim 16\%$ at 350 Hz	$< 1\%$ at 3 kHz
Performance		
Trigger Rate	350 Hz (stereo)	3 kHz
Trigger Threshold	$100\,\mathrm{GeV}$	$\sim$ 15–25 GeV

Table 1: Comparison of modified / improved characteristics between H·E·S·S·-I and the VLCT.